HHS Public Access

Author manuscript

ACS Appl Mater Interfaces. Author manuscript; available in PMC 2019 October 18.

Published in final edited form as:

ACS Appl Mater Interfaces. 2017 December 13; 9(49): 42633–42638. doi:10.1021/acsami.7b15302.

Kinetics and Chemistry of Hydrolysis of Ultrathin, Thermally Grown Layers of Silicon Oxide as Biofluid Barriers in Flexible Electronic Systems

Yoon Kyeung Lee[†,‡,#], **Ki Jun Yu**[§,#], **Yerim Kim**[‡], **Younghee Yoon**[‡], **Zhaoqian Xie**[⊥,●], **Enming Song**[‡,‖], **Haiwen Luan**[⊥], **Xue Feng**[●], **Yonggang Huang**[⊥], **John A. Rogers**[*,■]

[†]Department of Chemistry, Frederick Seitz Materials Research Laboratory, University of Illinois at Urbana–Champaign, Urbana, Illinois 61801, United States

[‡]Department of Materials Science and Engineering, Frederick Seitz Materials Research Laboratory, University of Illinois at Urbana–Champaign, Urbana, Illinois 61801, United States

[§]Department of Electrical and Electronic Engineering, Yonsei University, Seoul 03722, Republic of Korea

[‖]Department of Materials Science, Fudan University, Shanghai 200433, P.R. China

[⊥]Department of Civil and Environmental Engineering, Mechanical Engineering, and Materials Science and Engineering, McCormick School of Engineering, and Feinberg School of Medicine, Northwestern University, Evanston, Illinois 60208, United States

[■]Center for Bio-Integrated Electronics, Departments of Materials Science and Engineering, Biomedical Engineering, Chemistry, Mechanical Engineering, Electrical Engineering and Computer Science, and Neurological Surgery, Simpson Querrey Institute for Nano/biotechnology, McCormick School of Engineering, and Feinberg School of Medicine, Northwestern University, Evanston, Illinois 60208, United States

[●]AML, Department of Engineering Mechanics, Center for Mechanics and Materials, Tsinghua University, Beijing 100084, China

Abstract

Flexible electronic systems for bioimplants that offer long-term (multidecade) stability and safety in operation require thin, biocompatible layers that can prevent biofluid penetration. Recent work shows that ultrathin films of silicon dioxide thermally grown (TG-SiO_2) on device-grade silicon wafers and then released as transferrable barriers offer a remarkable set of attributes in this context. This paper examines the chemical stability of these materials in aqueous solutions with different combinations of chemistries that are present in biofluids. Systematic measurements

[*]Corresponding Author jrogers@northwestern.edu.

[#]These authors contributed equally to this work (Y.K.L. and K.J.Y.).

The manuscript was written through contributions of all authors. All authors have given approval to the final version of the manuscript.

Supporting Information

The Supporting Information is available free of charge on the ACS Publications website at DOI: 10.1021/acsami.7b15302.

Table and figures that summarize the chemical composition of the simulated biofluids; dissolution rates of TG-SiO_2 in Na_2HPO_4/NaH_2PO_4, NaCl, and KCl solutions (PDF)

The authors declare no competing financial interest.

reveal the dependence of the dissolution rate of TG-SiO_2 on concentrations of cations (Na^+, K^+, Mg^{2+}, Ca^{2+}) and anions (Cl^-,HPO_4^{2-}) at near-neutral pH. Certain results are consistent with previous studies on bulk samples of quartz and nanoparticles of amorphous silica; others reveal significant catalyzing effects associated with divalent cations at high pH and with specific anions at high ionic strength. In particular, Ca^{2+} and HPO_4^{2-} greatly enhance and silicic acid greatly reduces the rates. These findings establish foundational data of relevance to predicting lifetimes of implantable devices that use TG-SiO_2 as biofluid barriers, and of other classes of systems, such as environmental monitors, where encapsulation against water penetration is important.

Graphical Abstract:

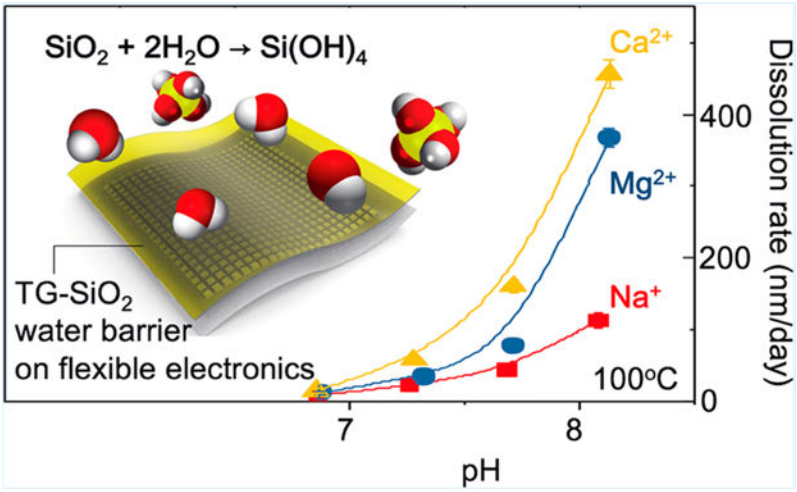

Keywords

thermal oxide; water barrier; silica dissolution; encapsulation; flexible electronics

1. INTRODUCTION

Recent advances in high-performance, flexible electronic/optoelectronic devices establish the foundations for physiological monitors and therapeutic systems capable of implantation in nearly any region of the body.[1–9] Examples range from devices for high-resolution electrophysiological mapping on the cardiac surfaces to injectable needles for optical stimulation and/or pharmacological manipulation of targeted neural circuits.[1,3] Because of the intrinsically low bending stiffnesses of the thin materials used in these platforms, such devices can establish conformal, minimally invasive interfaces to the curved, dynamic surfaces of soft biological systems while possessing many of the performance characteristics associated with rigid, planar, semiconductor-wafer-based integrated circuits. The absence of thin, flexible film barriers to biofluids has been a critical obstacle for use of such platforms as chronic implants, where the ultimate time scale for stable operation may reach into the realm of many decades. Recent work shows that physically transferred layers of silicon dioxide (TG-SiO_2) thermally grown on device-grade silicon wafers can provide defect-free isolation from biofluids without significantly compromising the flexible mechanics, suitable

for integration onto broad classes of biocompatible electronic devices.[10,11] The dense, amorphous consolidated nature of the TG-SiO_2 and its nearly perfect nature (e.g., pinhole-free) follow from the controlled, high-temperature growth conditions and the single-crystalline, atomically smooth growth substrates. The resulting films can enable zero water penetration across macroscopic areas even at thicknesses in the range of only tens to hundreds of nanometers, thereby extending the use of this material beyond applications as a thin film dielectric or a flat substrate for small particle growth.[12,13] The ultimate failure mode is in gradual reductions in thickness caused by dissolution of SiO_2 through hydrolysis ($SiO_2 + 2H_2O \rightarrow Si(OH)_4$) associated with immersion in biofluids.[10] The rate of this dissolution and its dependence on chemical composition of the surrounding aqueous solution therefore represent issues of critical importance in selecting designs to match lifetime requirements.

Previous studies show that the thickness of TG-SiO_2 decreases in a linear fashion with time in near neutral aqueous buffer solutions such as phosphate buffered saline (PBS) at rates of 10^{-2} to 10^2 nm/day in a temperature range from 25 to 100 °C, with Arrhenius scaling.[10,14] Thermal oxides formed using wet oxidation show slightly higher rates of dissolution compared to those formed by dry oxidation (by ~5%), consistent with their lower density.[14] The results suggest that the hydrolysis of TG-SiO_2 proceeds by surface reactions without a significant role of reactive diffusion of water into the bulk SiO_2 or of water permeation through defect sites. The studies reported here focus on detailed, parametric investigations of the effects of the chemical composition of the surrounding solution, to establish essential aspects of the hydrolysis reaction and its role in determining the stability of implantable flexible electronic devices. As described in the following, the findings indicate that the compositional variance of different types of simulated biofluids (PBS, Hank's balanced solution with and without Mg^{2+} and Ca^{2+}, and artificial perspiration) can alter the dissolution rates to a significant degree. Silicic acid, another ubiquitous chemical in biofluids, can strongly decelerate the dissolution, depending on the concentration. Measurements of TG-SiO_2 dissolution in aqueous solutions with various types of ions (Na^+, K^+, Ca^{2+}, Mg^{2+}, Cl^-, HPO_4^{2-}), ionic strengths (0−1 M), and pH (6−9) reveal accelerated dissolution at high ionic concentrations for all ion types, but with different acceleration factors and saturation levels. At similar ionic strength and pH, Ca^{2+} catalyzes the dissolution more effectively than monovalent cations (Na^+, K^+) and Mg^{2+}, especially at higher pH. HPO_4^{2-} leads to rates of dissolution that are faster than those associated with Cl^- at higher ionic strength. The discussion summarizes these results and compares them to previous studies of dissolution kinetics with other forms of silica such as quartz and amorphous polymorphs, with emphasis on underlying mechanistic reasoning.

2. RESULTS AND DISCUSSION

Figure 1a shows optical images of a piece of flexible electronics with four n-type metal-oxide-semiconductor (NMOS) transistors covered with an ultrathin layer of TG-SiO_2 (900 nm) for encapsulation. Transfer characteristics of a representative transistor are in Figure 1b in a log scale at a supply voltage V_{DS} = 0.1 V. Soaking these transistors in phosphate buffered saline (PBS, pH 7.4) at 100 °C accelerates the rate of hydrolysis of TG-SiO_2. The on/off current ratio remains ~10^8 before a sudden failure at day 10 due to the complete

dissolution of the TG-SiO_2 and subsequent exposure of the transistor to water. Figure 1c,d summarizes observations of spatially uniform thinning of layers of TG-SiO_2 by hydrolysis in simulated biofluids. The measurements involve immersing 5 mm × 5 mm pieces of Si wafer with a ~300 nm thick layer of TG-SiO_2 in 30 mL of each solution. Calculations based on the amount of dissolved SiO_2 and direct experimental measurements by inductively coupled plasma mass spectrometry analysis indicate that the silicic acid concentration remains <1 ppm throughout the course of these experiments. Figure 1c summarizes the changes in thickness associated with immersion in five types of simulated biofluids at 37 °C: PBS, Hank's balanced saline solution (HBSS) with and without Mg^{2+} and Ca^{2+}, artificial perspiration, and bovine serum. Table S1 (Supporting Information) summarizes the compositional differences of these solutions. The main difference between perspiration, PBS, and HBSS is in their pH levels (PBS, 7.4; HBSS, 8.3 (CO_2-sensitive); perspiration, 4.5). The viscosity of the serum is higher by ~10% compared to other solutions due to its protein content. Each solution yields a different dissolution rate: <0.01 nm/day (perspiration); 0.07 ± 0.02 nm/day (PBS);0.46 ± 0.03 nm/day (HBSS without Mg^{2+}, Ca^{2+}); 1.26 ± 0.02 nm/day (HBSS with Mg^{2+}, Ca^{2+}) (Figure 1d). The rates increase with pH, consistent with previous reports.[14] Adding Mg^{2+} (0.9 mM) and Ca^{2+} (1.3 mM) to HBSS increases the rate by a factor of nearly 3. Binding of proteins in bovine serum to the surface of the TG-SiO_2 leads to an apparent increase in thickness, thereby frustrating an accurate measurement of dissolution. Prior studies show that proteins irreversibly adsorb on silica surface at room temperature, with an order of 10^{-1} $\mu g/cm^2$.[15,16]

Optical images in Figure 2a highlight the changes in color that occur as the thickness of TG-SiO_2 decreases in phosphate buffer solution (Na_2HPO_4/NaH_2PO (NaPO) 10 mM, pH7.4) at 100 °C. (Here, the molar concentration of the phosphate buffer is the sum of NaH_2PO_4 and Na_2HPO_4 as conventionally used in the buffer description.) The uniformity in color during the dissolution is consistent with a high level of macroscopic uniformity in the hydrolysis reactions across the entire spatial extent of the sample. Figure 2b summarizes corresponding reflectance data that show a continuous shift of the peaks toward shorter wavelengths as the thickness decreases. Such measurements quantify the changes in thickness (from 320 nm at 0 h to 210 nm at 24 h) to yield the dissolution rate. Parametric studies at an elevated temperature (100 °C) yield data on the dependence of dissolution rate on ion concentration and pH. Biological and environmental fluids cover a range of pH values and concentrations of ions. For example, the pH of common natural water can be as low as 4.5 (urine, sweat) and as high as 8.4 (seawater). In terms of salinity, rivers and oceans contain 0.1 g to 100g/L solid contents mostly associated with dissolved cations (Na^+, Mg^{2+}, and Ca^{2+}) and anions (Cl^-, HCO^-_3, SO_4^{2-}, and silica) while extracellular biofluids contain strictly regulated amounts of salts within 8−20 g/L, mostly NaCl. Figure 2c summarizes the catalyzing effect of ions (NaCl) at various pH levels adjusted by ~3.3 mM NaPO. Since the ratio between NaH_2PO_4 and Na_2HPO_4 in phosphate buffer changes depending on the pH, we used formulations with constant ionic strength (IS, 10 mM NaPO), not concentration, for all pH values. The results show that at all NaCl concentrations (30, 140, and 990 mM), the dissolution rates increase with pH with a half-order dependence on OH^- concentration, consistent with previous studies of TG-SiO_2 in phosphate buffer solution.[10] Rates are as follows: 40 ± 3 nm/day (30 mM), 46 ± 3 nm/day (140 mM), and 64 ± 4 nm/day (990 mM) at

pH ~6.9; 218 ± 6 nm/day (30 mM), 260 ± 8 nm/day (140 mM), and 359 ± 8 nm/day (990 mM) at pH 8.2 (990 mM) to pH 8.4 (30 and 140 mM). The enhanced dissolution at high pH likely follows from deprotonation of the silanol groups on the silica surface and their enhanced reactivity toward hydrolysis, as observed in the relation between the silica surface charge and the dissolution rates for other types of silica.[17] Although atomistic mechanisms of the accelerating effect of ions are not well understood, experimental results suggest that the presence of ions increases the frequency of the reactions without significantly decreasing the activation energy.[18] Consistent with those prior results, the apparent activation energies for the hydrolysis of TG-SiO_2 extracted from measurements at three temperatures with Arrhenius scaling suggests that the average activation energies remain ~0.89 eV without significant differences between solutions with different ion concentrations (Figure S1). This value is similar to those for amorphous silica (0.85 eV for fused quartz and 0.79 eV for pyrolyzed silica).[19]

Although studies of dissolution in pure water with <1 ppm of $Si(OH)_4$ yield valuable kinetics information, investigations of dissolution in solutions with specified, non-negligible concentrations of $Si(OH)_4$ are important in the context of biological environments. Figure 3 shows the effects of silicic acid ($Si(OH)_4$), a product of SiO_2 hydrolysis and a ubiquitous presence in biological aqueous systems, typically at the 10^0 to 10^1 ppm level. The formulations used $Si(OH)_4$ extracted from a 1000 ppm of Si standard solution (Sigma-Aldrich). The data in Figure 3a highlight the strong decrease of dissolution rate with increase in [$Si(OH)_4$] due to an increased rate of the reverse hydrolysis reaction, consistent with the dissolution behavior of quartz and other silica polymorphs.[20–22] The dissolution almost entirely stops at ~600 ppm of $Si(OH)_4$ at 100 °C.

Figure 3b presents fits of experiment data to a polynuclear dissolution model previously used to explain the dissolution of fused quartz/synthetic silica in solutions containing $Si(OH)_4$.[22] This model describes the dependence of SiO_2 dissolution on [$Si(OH)_4$] by reduced rates of net detachment of $Si(OH)_4$ from the surface and increased activation energy for vacancy (or highly reactive site) formation where dissolution starts to spread. Specifically, the reactive sites refer to the surface silica tetrahedra with coordination numbers lower than those of bulk SiO_2, thereby yielding high surface energy. The model expresses the rate as

$$\ln R = \ln(hSA) - \frac{\pi\alpha^2\omega h}{(kT)^2}\frac{1}{|\sigma|}$$

where R is the volume of dissolution nuclei formed per unit area of surface and time, h is the height of the vacancy, S is the surface area affected by each nucleation event, A is a pre-exponential factor for nucleation rate, ω is the specific volume of molecule (cm^3/molecule), α is the local interfacial free energy, k is the Boltzmann constant, and T is the temperature.[22] $\sigma = \ln(C/Ce)$ is the degree of undersaturation, where C and Ce (630 ppm) are experimental and equilibrium concentrations of $Si(OH)_4$, respectively. The equation indicates that the logarithm of the rate of removing a unit of material from the surface has a squared dependence on the interfacial free energy (α) to create a new surface with highly reactive Si

atoms exposed. We used these values for the following parameters, $\omega_{TG-SiO2} = 4.54^{-23}$ cm/molecule, height $h_{TG-SiO2}$ =2.17 Å, and T = 373.15 K.[22] The polynuclear model applies to dissolution processes dominated by the detachment of SiO_2 units around nucleated reactive sites. The lines in Figure 3b show the model fit to the experiment data of TG-SiO_2 dissolution. The interfacial free energy $\alpha_I^* = 80.2$ mJ/m^2 is obtained for the higher-slope region at high undersaturation, and $\alpha_{II}^* = 29.3$ mJ/m^2 is obtained for the lower-slope region close to saturation. The interfacial energies of TG-SiO_2 are similar to the those of quartz, where two different slopes have been attributed to different regimes of the dissolution dominated either by nucleation of reactive surface Si atoms with fewer backbonds (undersaturation) or by reactive surface silicon atoms intrinsically present in the original structure (close to saturation).[22]

Since ions can accelerate the rates of dissolution (Figure 2c), studies of different cation and anion types that are present in biological or groundwater are important. Figure 4 summarizes the role of cation type. Here, the use of Tris buffer instead of phosphate buffer prevents precipitation reactions from interactions of divalent cations (Ca^{2+} and Mg^{2+}) with the HPO_4^{2-}. Figure 4a shows measured rates in $CaCl_2$, $MgCl_2$, and NaCl solutions at 30 mM ionic strength (IS) and near neutral pH. The results show that Ca^{2+} accelerates the dissolution more effectively than Mg^{2+} and Na^+ in all pH ranges, as previously reported at low silicic acid concentrations.[21,22] The differences between Mg^{2+} and Na^+ are insignificant for pH in the low part of this range (9 ± 4 nm/day (NaCl), 13 ± 3 nm/day ($MgCl_2$), and 15 ± 3 nm/day ($CaCl_2$) at pH 6.9), but become significant at higher pH (114 ± 11 nm/day (NaCl), 367 ± 13 nm/day ($MgCl_2$), and 456 ± 20 nm/day ($CaCl_2$) at pH 8.1). The underlying mechanisms likely relate to enhanced electrostatic interactions between more negatively charged SiO_2 surfaces and divalent cations at higher pH.[17,23] Since the [Cl^-] is lower in $CaCl_2$ and $MgCl_2$ solutions than that in the NaCl solution at the same ionic strength, the observed acceleration can be attributed to the cations. The results are consistent with previous studies on quartz where faster rates occur with Ca^{2+} than with Mg^{2+}.[24] Previous ab initio calculations suggest a quantum mechanical origin for the role of cations in accelerated dissolution of SiO_2. Here, bond paths can form between the divalent cations and bridging oxygen sites with partial negative charges on the silica surface.[25] This interaction weakens the surrounding Si−O bonds and enhances the susceptibility of the Si atoms to attack by water. According to these computational results, the differences between Ca^{2+} and Mg^{2+} arise from differences in water dynamics associated with these ions. Dissolution rates in KCl and NaCl solutions are similar (Figure S2).

Figure 4b presents the previous results in units of mol/s·cm^2 to facilitate comparisons with the rates associated with quartz and other amorphous forms of silica. The observed rates, 10^{-12}–10^{-11} mol/s·cm^2 at near neutral pH at 100 °C are all comparable for similar conditions: quartz, 10^{-15}–10^{-14} mol/s· cm^2 at 70 °C and 10^{-11}–10^{-10} mol/s·cm^2 at 200 °C;[26,17] amorphous silica, 10^{-11} at 150 °C.[22] The reaction order on pH, which is independent of the units, is 0.88, 1.13, and 1.14 for Na^+, Mg^{2+}, and Ca^{2+}, respectively, in Tris buffer. This dependence on pH is significantly larger than that for phosphate buffered solutions (0.5) as the values of the pH dependence depend on the buffer systems.[18] The difference between phosphate and Tris buffers could result from interactions between the phosphate anion and the SiO_2 surface, as discussed later in the context of studies of effects of anions (Figure 5).

Figure 4c describes the dependence of dissolution rates on the ionic strength at pH 7.7. The rate associated with Ca^{2+} is the highest at all concentrations. For all ion types, the rates increase initially at low concentrations, and then tend to saturate at high concentrations (from 13 ± 5 nm/day (without salts) to 166 ± 10 nm/day (NaCl), 164 ± 16 nm/day ($MgCl_2$), and 437 ± 22 nm/day ($CaCl_2$) at 1 M ionic strength, pH 7.7). This saturation behavior also occurs with quartz,[19] and is generally believed to result from saturation of cations near the SiO_2 surface after effective screening of the negative SiO_2 surface charge.

Although the enhancements of dissolution rates in electrolyte solutions are typically attributed to cation−SiO_2 and cation−water interactions,[27,24] anion specificity can be observed in the case of Cl^- and HPO_4^{2-}. Figure 5 compares dissolution rates in solutions of NaCl and Na_2HPO_4. The Na_2HPO_4 solutions also include a small amount of NaH_2PO_4 (Na_2HPO_4/NaH_2PO_4 <0.1) to adjust the solution pH while maintaining the total ionic strength at the desired level. Addition of 10 mM (by ionic strength) Na_2HPO_4/NaH_2PO_4 (NaPO) to the NaCl solutions maintains a constant pH. Figure 5a compares the concentration of Na^+ in the NaCl and NaPO solutions at ionic strengths of 40 mM, 150 mM, and 1 M. In all cases, [Na^+] is higher in NaCl solutions than in NaPO solutions at the same ionic strength. Figure 5b,c summarizes dissolution rates in NaCl and NaPO solutions at different ionic strengths. The results indicate that the difference in the dissolution rates with different anions is small at 40 mM (e.g., 40 ± 3 nm/day (NaCl) and 40 ± 4 nm/day (NaPO) at pH 6.9) but that the rates with phosphate anions become significantly faster than those with Cl^- at high ionic strengths for all pH levels (e.g., at pH 6.8, 46 ± 3 nm/day (NaCl) and 77 ± 3 nm/day (NaPO) in 150 mM and 64 ± 7 nm/day (NaCl) and 146 ± 9 nm/day (NaPO) in 1 M ionic strength). Such anion-specific dissolution behaviors may arise from screening of negative surface charge of SiO_2 by Na^+ at high ionic strength and direct interaction between SiO_2 and anions. Strong hydrogen-bonding interactions between phosphate and the silica surface can be observed in sum frequency generation and FTIR spectroscopy.[28,29] Measurements of dissolution at different temperatures (Figure S3) suggest an activation energy with HPO_4^{2-} (0.6 eV) that is lower than that with Cl^- (0.8 eV) at 150 mM ionic concentration, thereby suggesting accelerating mechanisms that are different than those of cations.

3. CONCLUSION

This paper summarizes the results of systematic studies of the dissolution behaviors of ultrathin layers of TG-SiO_2 in aqueous solutions with compositions relevant to those in biofluids. The data reveal key factors in the dissolution kinetics: ion type and concentration, pH, and concentration of silicic acid. Some of the findings are consistent with the previous studies on quartz and amorphous silica. Additional results establish significant catalyzing effects from divalent cations at high pH and anion-specific features at high ionic strength. The insights into these chemistries are critically important in the context of the use of TG-SiO_2 as a water barrier layer for active, flexible electronic implants, and in other cases where long-term survivability is necessary in aqueous environments.

4. EXPERIMENTAL METHODS

The fabrication process for flexible NMOS transistors began with the isolation of silicon transistors on an SOI wafer (200 nm top Si/1 μm buried thermal oxide, SOITEC). Solid source doping with phosphorus yielded source and drain contacts at concentration level of ~10^{19} cm^{-3} with a channel length of 20 μm and width of 600 μm. Thermal oxidation and atomic layer deposition (ALD) yielded a dielectric stack of thermal SiO_2 (30 nm)/Al_2O_3 (13 nm) at ~1150 and 80 °C, respectively. A layer of Cr/Au (5 nm/100 nm) served as source, drain, gate electrodes, and metal interconnects. A transfer process bonded the front side of this substrate to a thin polymer film (Kapton, DuPont, 13 μm) laminated onto a glass substrate coated with a layer of dimethylsiloxane (PDMS; 10 μm) as a temporary support. The bonding involved application of a commercial adhesive (Kwik-Sil, World Precision Instruments). Reactive ion etching (RIE) with SF_6/O_2 (Plasma Therm) followed by inductively coupled plasma RIE (ICP-RIE, Surface Technology System) with SF_6 exposes the surface of the TG-SiO_2 (~900 nm, thinned by 100 nm during the etching process) as a biofluid barrier and biointerface. Peeling the device away from the substrate completed the process.

All dissolution experiments used commercially obtained Si wafers (P-type (Boron), 1−100 Ω·cm, (100), University Wafer). TG-SiO_2 was grown by wet thermal oxidation (1150 °C) on their surfaces. Soaking tests involved various types of simulated biofluids including PBS (Corning cellgro), Hank's balanced salt solution (HBSS) (Thermo Fisher Scientific), bovine serum (RMBIO), and artificial perspiration (Pickering Laboratories) at 37 °C. Storage of these solutions occurred in PETE bottles, as purchased; experiments used high-density polyethylene (HDPE) bottles (United States Plastic Corp.). NaCl, KCl, and NaH_2PO_4/Na_2HPO_4 solutions were prepared by mixing the salts in deionized water. $CaCl_2$ and $MgCl_2$ solutions were diluted from their 1 M standard solution (Sigma-Aldrich). Si standard solution (1 g/L; Sigma-Aldrich) prepared by dissolving Si in 2% NaOH was added to PBS to include silicic acid. The pH of phosphate buffer was adjusted by changing the ratio between NaH_2PO_4 and Na_2HPO_4 while pH of Tris buffer was adjusted by adding HCl. After the soaking tests at 37 or 100 °C in each solution, the thickness of the TG-SiO_2 was measured by a reflectometer (MProbe, Semicon Soft). Dissolution rates indicated in the plots correspond to average values calculated from measurements on three separate pieces of TG-SiO_2.

Supplementary Material

Refer to Web version on PubMed Central for supplementary material.

ACKNOWLEDGMENTS

Y. K. Lee is thankful for the support from Kwanjeong Educational Foundation. K. J. Yu acknowledges the support from the National Research Foundation of Korea (NRF 2017M1A2A2048904). Z.X. and X.F. acknowledge the support from the National Basic Research Program of China (Grant No. 2015CB351900) and National Natural Science Foundation of China (Grant Nos. 11402134 and 11320101001). Y.H. acknowledges the support from NSF (Grant Nos. 1400169, 1534120, and 1635443) and NIH (Grant No. R01EB019337).

REFERENCES

(1). Kim T; McCall JG; Jung YH; Huang X; Siuda ER; Li Y; Song J; Song YM; Pao HA; Kim R-H; Lu C; Lee SD; Song I-S; Shin G; Al-Hasani R; Kim S; Tan MP; Huang Y; Omenetto FG; Rogers JA; Bruchas MR Injectable, Cellular-Scale Optoelectronics with Applications for Wireless Optogenetics. Science 2013, 340 (6129), 211–216. [PubMed: 23580530]

(2). Kim D-H; Ahn J-H; Choi WM; Kim H-S; Kim T-H; Song J; Huang YY; Liu Z; Lu C; Rogers JA Stretchable and Foldable Silicon Integrated Circuits. Science 2008, 320 (5875), 507–511. [PubMed: 18369106]

(3). Yu KJ; Kuzum D; Hwang S-W; Kim BH; Juul H; Kim NH; Won SM; Chiang K; Trumpis M; Richardson AG; Cheng H; Fang H; Thompson M; Bink H; Talos D; Seo KJ; Lee HN; Kang S-K; Kim J-H; Lee JY; Huang Y; Jensen FE; Dichter MA; Lucas TH; Viventi J; Litt B; Rogers JA Bioresorbable Silicon Electronics for Transient Spatiotemporal Mapping of Electrical Activity from the Cerebral Cortex. Nat. Mater 2016, 15 (7), 782–791. [PubMed: 27088236]

(4). Someya T; Kato Y; Sekitani T; Iba S; Noguchi Y; Murase Y; Kawaguchi H; Sakurai T Conformable, Flexible, Large-Area Networks of Pressure and Thermal Sensors with Organic Transistor Active Matrixes. Proc. Natl. Acad. Sci. U. S. A 2005, 102 (35), 12321–12325. [PubMed: 16107541]

(5). Xu L; Gutbrod SR; Bonifas AP; Su Y; Sulkin MS; Lu N; Chung H-J; Jang K-I; Liu Z; Ying M; Lu C; Webb RC; Kim J-S; Laughner JI; Cheng H; Liu Y; Ameen A; Jeong J-W; Kim G-T; Huang Y; Efimov IR; Rogers JA 3D Multifunctional Integumentary Membranes for Spatiotemporal Cardiac Measurements and Stimulation across the Entire Epicardium. Nat. Commun 2014, 5, 3329. [PubMed: 24569383]

(6). Jeong J-W; Yeo W-H; Akhtar A; Norton JJS; Kwack Y-J; Li S; Jung S-Y; Su Y; Lee W; Xia J; Cheng H; Huang Y; Choi W-S; Bretl T; Rogers JA Materials and Optimized Designs for Human-Machine Interfaces Via Epidermal Electronics. Adv. Mater 2013, 25 (47), 6839–6846. [PubMed: 24327417]

(7). Rogers JA; Someya T; Huang Y Materials and Mechanics for Stretchable Electronics. Science 2010, 327 (5973), 1603–1607. [PubMed: 20339064]

(8). Jang K-I; Li K; Chung HU; Xu S; Jung HN; Yang Y; Kwak JW; Jung HH; Song J; Yang C; Wang A; Liu Z; Lee JY; Kim BH; Kim J-H; Lee J; Yu Y; Kim BJ; Jang H; Yu KJ; Kim J; Lee JW; Jeong J-W; Song YM; Huang Y; Zhang Y; Rogers JA Self-Assembled Three Dimensional Network Designs for Soft Electronics. Nat. Commun 2017, 8, 15894. [PubMed: 28635956]

(9). Lee YK; Jang K-I; Ma Y; Koh A; Chen H; Jung HN; Kim Y; Kwak JW; Wang L; Xue Y; Yang Y; Tian W; Jiang Y; Zhang Y; Feng X; Huang Y; Rogers JA Chemical Sensing Systems That Utilize Soft Electronics on Thin Elastomeric Substrates with Open Cellular Designs. Adv. Funct. Mater 2017, 27 (9), 1605476.

(10). Fang H; Zhao J; Yu KJ; Song E; Farimani AB; Chiang C-H; Jin X; Xue Y; Xu D; Du W; Seo KJ; Zhong Y; Yang Z; Won SM; Fang G; Choi SW; Chaudhuri S; Huang Y; Alam MA; Viventi J; Aluru NR; Rogers JA Ultrathin, Transferred Layers of Thermally Grown Silicon Dioxide as Biofluid Barriers for Biointegrated Flexible Electronic Systems. Proc. Natl. Acad. Sci. U. S.A 2016, 113 (42), 11682–11687. [PubMed: 27791052]

(11). Fang H; Yu KJ; Gloschat C; Yang Z; Song E; Chiang C-H; Zhao J; Won SM; Xu S; Trumpis M; Zhong Y; Han SW; Xue Y; Xu D; Choi SW; Cauwenberghs G; Kay M; Huang Y; Viventi J; Efimov IR; Rogers JA Capacitively Coupled Arrays of Multiplexed Flexible Silicon Transistors for Long-Term Cardiac Electrophysiology. Nat. Biomed. Eng 2017, 1, 0038. [PubMed: 28804678]

(12). Wakayama Y; Tagami T; Tanaka S Three-dimensional islands of Si and Ge formed on SiO_2 through crystallization and aggromeration from amorphous thin films. Thin Solid Films 1999, 350, 300.

(13). Nakamura Y; Watanabe K; Fukuzawa Y; Ichikawa M Observation of the quantum-confinement effect in individual Ge nanocrystals on oxidized Si substrates using scanning tunneling spectroscopy. Appl. Phys. Lett 2005, 87, 133119.

(14). Kang SK; Hwang SW; Cheng H; Yu S; Kim BH; Kim JH; Huang Y; Rogers JA Dissolution Behaviors and Applications of Silicon Oxides and Nitrides in Transient Electronics. Adv. Funct. Mater 2014, 24 (28), 4427–4434.

(15). Nakanishi K; Sakiyama T; Imamura K REVIEW On the Adsorption of Proteins on Solid Surfaces, a Common but Very Complicated Phenomenon. J. Biosci. Bioeng 2001, 91 (3), 233–244. [PubMed: 16232982]

(16). Catalano F; Alberto G; Ivanchenko P; Dovbeshko G; Martra G Effect of Silica Surface Properties on the Formation of Multilayer or Submonolayer Protein Hard Corona: Albumin Adsorption on Pyrolytic and Colloidal SiO2 Nanoparticles. J. Phys. Chem. C 2015, 119, 26493–26505.

(17). Brady PV; Walther JV Kinetics of Quartz Dissolution at Low Temperatures. Chem. Geol 1990, 82, 253–264.

(18). Dove PM; Crerar DA Kinetics of Quartz Dissolution in Electrolyte Solutions Using a Hydrothermal Mixed Flow Reactor. Geochim. Cosmochim. Acta 1990, 54 (4), 955–969.

(19). Icenhower JP; Dove PM The Dissolution Kinetics of Amorphous Silica into Sodium Chloride Solutions: Effects of Temperature and Ionic Strength. Geochim. Cosmochim. Acta 2000, 64 (24), 4193–4203.

(20). Fleming BA Kinetics of Reaction between Silicic Acid and Amorphous Silica Surfaces in NaCl Solutions. J. Colloid Interface Sci 1986, 110 (1), 40–64.

(21). Dove PM; Han N; De Yoreo JJ Mechanisms of Classical Crystal Growth Theory Explain Quartz and Silicate Dissolution Behavior. Proc. Natl. Acad. Sci. U. S. A 2005, 102 (43), 15357–15362. [PubMed: 16230632]

(22). Dove PM; Han N; Wallace AF; De Yoreo JJ Kinetics of Amorphous Silica Dissolution and the Paradox of the Silica Polymorphs. Proc. Natl. Acad. Sci. U. S. A 2008, 105, 9903–9908. [PubMed: 18632576]

(23). Dove PM; Craven CM Surface Charge Density on Silica in Alkali and Alkaline Earth Chloride Electrolyte Solutions. Geochim. Cosmochim. Acta 2005, 69 (21), 4963–4970.

(24). Dove PM; Nix CJ The Influence of the Alkaline Earth Cations, Magnesium, Calcium, and Barium on the Dissolution Kinetics of Quartz. Geochim. Cosmochim. Acta 1997, 61 (16), 3329–3340.

(25). Wallace AF; Gibbs GV; Dove PM Influence of Ion-Associated Water on the Hydrolysis of Si-O Bonded Interactions. J. Phys. Chem. A 2010, 114 (7), 2534–2542. [PubMed: 20108957]

(26). Dove P The Dissolution Kinetics of Quartz in Sodium Chloride Solutions at 25 Degrees to 300 Degrees C. Am. J. Sci 1994, 294, 665–712.

(27). Azam MS; Weeraman CN; Gibbs-Davis JM Specific Cation Effects on the Bimodal Acid-Base Behavior of the Silica/water Interface. J. Phys. Chem. Lett 2012, 3 (10), 1269–1274. [PubMed: 26286770]

(28). Casillas-Ituarte NN; Chen X; Castada H; Allen HC Na^{+} and Ca^{2+} Effect on the Hydration and Orientation of the Phosphate Group of DPPC at Air − Water and Air − Hydrated Silica Interfaces. J. Phys. Chem. B 2010, 114 (29), 9485–9495. [PubMed: 20614879]

(29). Mao Y; Daniel LN; Whittaker N; Saffiotti U DNA Binding to Crystalline Silica Characterized by Fourier-Transform Infrared Spectroscopy. Environ. Health Perspect 1994, 102, 165–171.

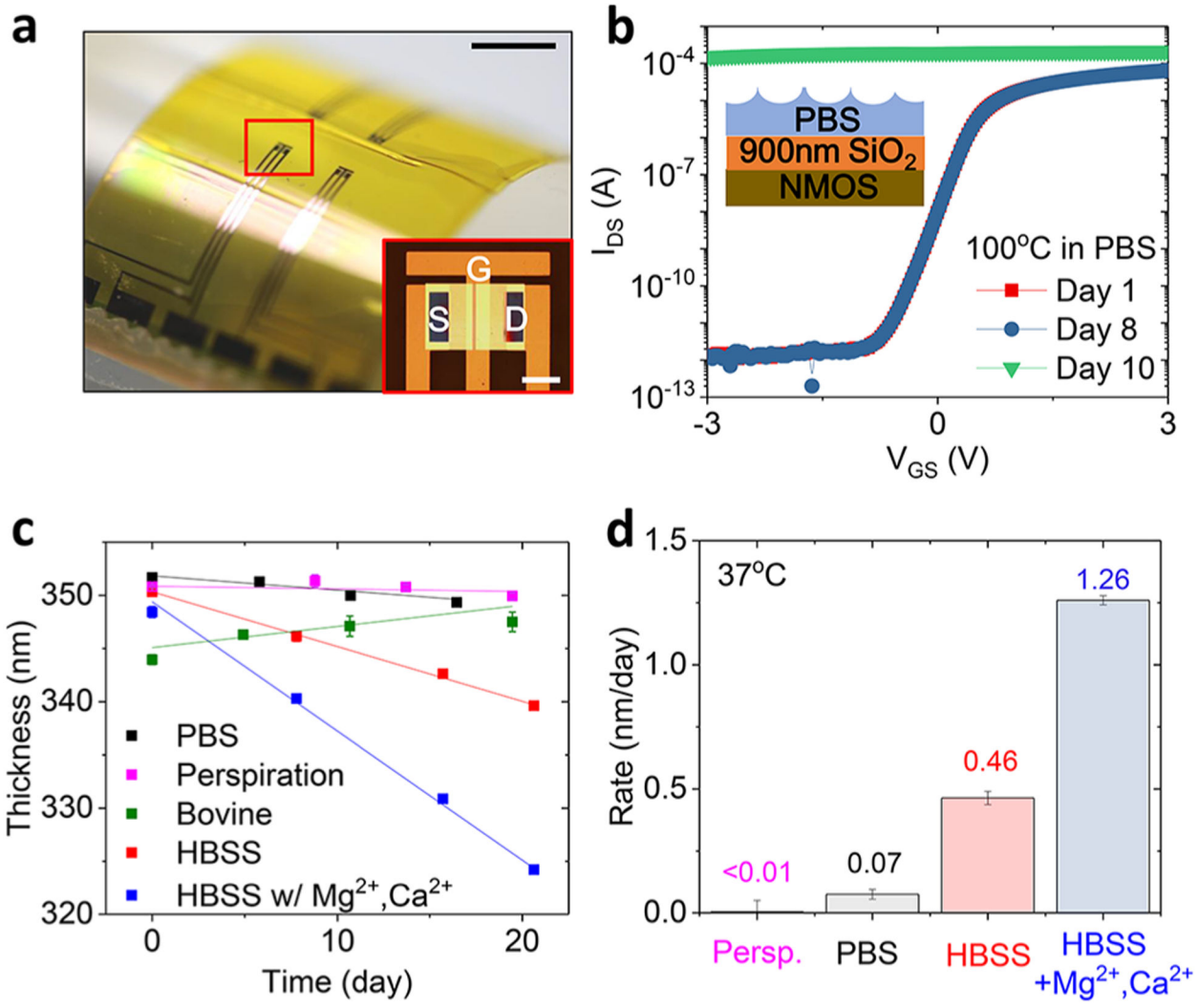

Figure 1.

Flexible electronics encapsulated with thermally grown silicon dioxide (TG-SiO_2) and dissolution of TG-SiO_2 due to immersion in simulated biofluids at 37 °C. (a, b) Demonstration of electronic devices and flexible electronic systems encapsulated with TG-SiO_2. (a) Optical images of flexible n-type metal-oxide-semiconductor (NMOS) transistors (scale bar: 1 cm (black), 200 μm (white, inset)). (b) Results of soak tests of NMOS in PBS solutions at 100 °C. (c) Change in thickness of TG-SiO_2 as a function of time of immersion in simulated biofluids. (d) Measured dissolution rates (nm/day) for these fluids.

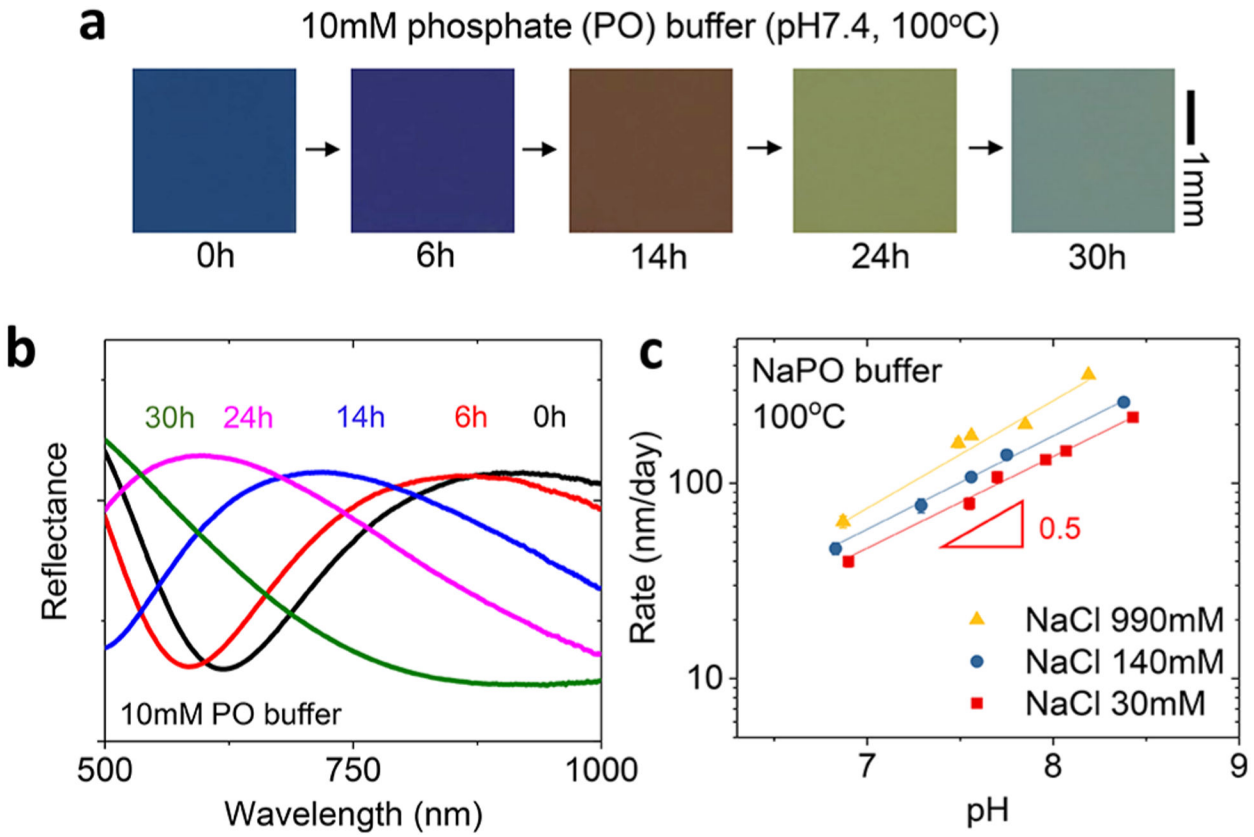

Figure 2.

Effects of ion concentration and pH on dissolution of $TGSiO_2$. (a) Optical images of $TG\text{-}SiO_2$ collected at several times of immersion in 10 mM sodium phosphate (Na_2HPO_4/NaH_2PO_4, NaPO) solution (pH 7.4) at 100 °C. (b) Reflectance curves at different times. (c) Effects of pH and NaCl concentration on the dissolution rate.

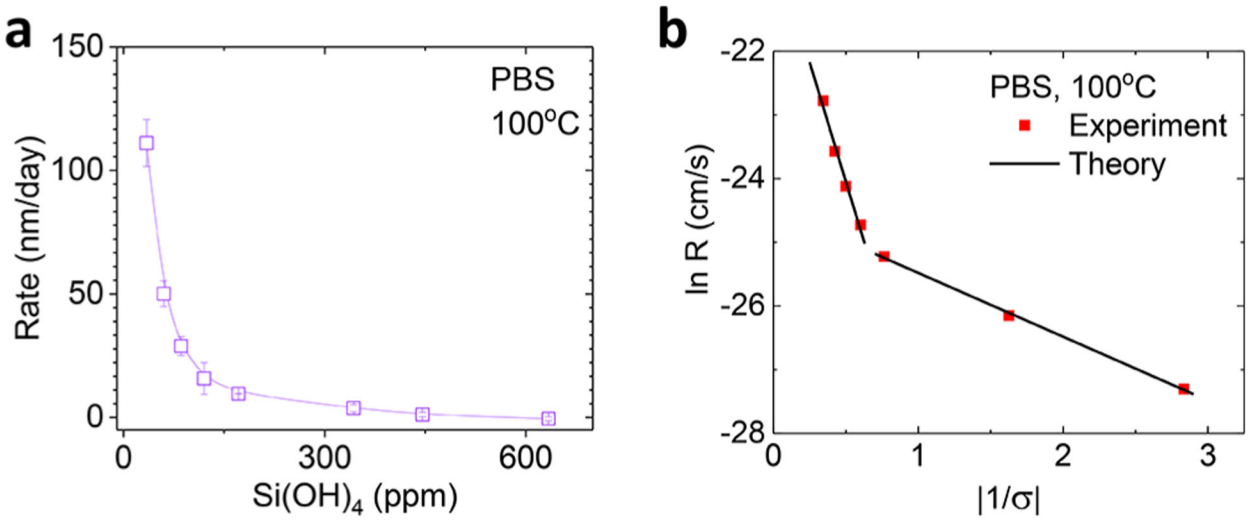

Figure 3.

Effects of silicic acid on dissolution of TG-SiO_2. (a) Effect of silicic acid concentration on dissolution rate in PBS. (b) Comparisons to a polynuclear dissolution model.

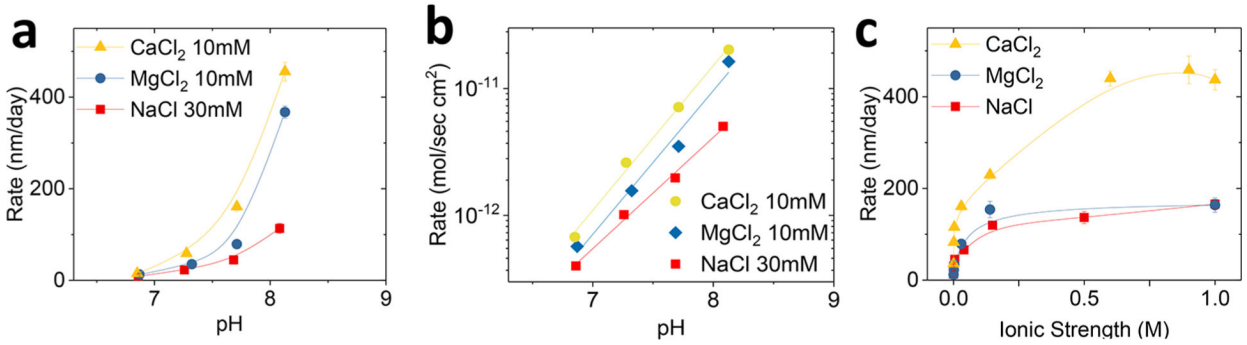

Figure 4.

Dependence of TG-SiO_2 dissolution on cation type. (a) Rate of dissolution in solutions of NaCl, $MgCl_2$, and $CaCl_2$ at different pH. (b) Dissolution rates in mol/s·cm^2. (c) Dissolution rates in solutions with different ionic strengths.

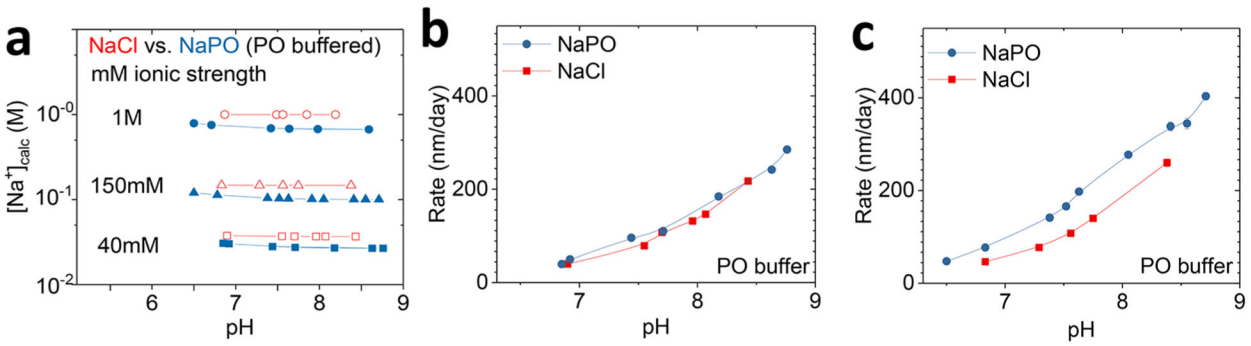

Figure 5.

Dependence of TG-SiO_2 dissolution on anion type. (a) Na^+ concentrations in solutions of NaCl and Na_2HPO_4/NaH_2PO_4 (NaPO). (b) Dissolution rates in solutions with 40 mM ionic strength. (c) Dissolution rates in solutions with 150 mM ionic strength.